
LOCALLY PERSISTENT EXPLORATION IN CONTINUOUS CONTROL TASKS WITH SPARSE REWARDS

Susan Amin*

Department of Computer Science, McGill University
Mila- Québec Artificial Intelligence Institute
susan.amin@mail.mcgill.ca

Maziar Gomrokchi*

Department of Computer Science, McGill University
Mila- Québec Artificial Intelligence Institute
maziar.gomrokchi@mail.mcgill.ca

Hossein Aboutaleb

Department of Computer Science, University of Waterloo
haboutal@uwaterloo.ca

Harsh Satija

Department of Computer Science, McGill University
Mila- Québec Artificial Intelligence Institute
harsh.satija@mail.mcgill.ca

Doina Precup

Department of Computer Science, McGill University
Mila- Québec Artificial Intelligence Institute
dprecup@cs.mcgill.ca

ABSTRACT

A major challenge in reinforcement learning is the design of exploration strategies, especially for environments with sparse reward structures and continuous state and action spaces. Intuitively, if the reinforcement signal is very scarce, the agent should rely on some form of short-term memory in order to cover its environment efficiently. We propose a new exploration method, based on two intuitions: (1) the choice of the next exploratory action should depend not only on the (Markovian) state of the environment, but also on the agent’s trajectory so far, and (2) the agent should utilize a measure of spread in the state space to avoid getting stuck in a small region. Our method leverages concepts often used in statistical physics to provide explanations for the behavior of simplified (polymer) chains, in order to generate persistent (locally self-avoiding) trajectories in state space. We discuss the theoretical properties of locally self-avoiding walks, and their ability to provide a kind of short-term memory, through a decaying temporal correlation within the trajectory. We provide empirical evaluations of our approach in a simulated 2D navigation task, as well as higher-dimensional MuJoCo continuous control locomotion tasks with sparse rewards.

1 Introduction

As reinforcement learning agents typically learn tasks through interacting with the environment and receiving reinforcement signals, a fundamental problem arises when these signals are rarely available. The sparsely distributed rewards call for a clever exploration strategy that exposes the agent to the unseen regions of the space via keeping track of the visited state-action pairs [1, 2]. However, that cannot be the case for high-dimensional continuous space-and-action spaces, as defining a notion of density for such tasks is intractable and heavily task-dependent [3, 4].

Here, we introduce an exploration algorithm that works independently of the extrinsic rewards received from the environment and is inherently compatible with continuous state-and-action tasks. Our proposed approach takes into account the agent’s short-term memory regarding the action trajectory, as well as the trajectory of the observed states in order to sample the next exploratory action. The main intuition is that in a pure exploration mode with minimal extrinsic reinforcement, the agent should plan trajectories that expand in the available space and avoid getting stuck in small regions. In other words, the agent may need to be “persistent” in its choice of actions; for example, in a locomotion task, an agent may want to pick a certain direction and maintain it for some number of steps, in order to ensure that it

*These authors contributed equally to the work

can move away from its current location, where it might be stuck at. The second intuition is that satisfying the first condition requires a notion of spread measure in the state space to warrant the agent’s exposure to unvisited regions. Moreover, in sparse reward settings, while the agent’s primary intention must be to avoid being trapped in local regions by maintaining a form of short-term memory, it must still employ a form of memory evaporation mechanism to maintain the possibility of revisiting the informative states. Note that in continuous state-and-action settings, modern exploration methods [5, 6, 7] fail to address the fore-mentioned details simultaneously.

Our polymer-based exploration technique (PolyRL) is inspired by the theory of freely-rotating chains (FRCs) in polymer physics to implement the aforementioned intuitions. FRCs describe the chains (collections of transitions or moves) whose successive segments are correlated in their orientation. This feature introduces a finite (short-term) stiffness (persistence) in the chain, which induces what we call *locally* self-avoiding walks (LSAWs). The strategy that emerges from PolyRL provides consistent movement, without the need for exact action repeats (*e.g.* methods suggested by [8, 9]), and can adapt the rigidity of the chain as required. Moreover, unlike action-repeat strategies, PolyRL is inherently applicable in continuous action-state spaces without the need to use any discrete representation of action or state space. The local self-avoidance property in a PolyRL trajectory cultivates an orientationally persistent move in the space while maintaining the possibility of revisiting the places visited before. In particular, in constructing LSAWs, PolyRL selects persistent actions in the action space and utilizes a measure of spread in the state space, called the *radius of gyration*, to maintain the (orientational) persistence in the chain of visited states. The PolyRL agent breaks the chain and performs greedy action selection once the correlation between the visited states breaks. The next few exploratory actions that follow afterward, in fact, act as a perturbation to the last greedy action, which consequently preserves the orientation of the greedy action. This feature becomes explicitly influential after the agent is exposed to some reinforcement, and the policy is updated, as the greedy action guides the agent’s movement through the succeeding exploratory chain of actions.

2 Notation and Problem Formulation

We consider the usual MDP setting, in which an agent interacts with a Markov Decision Process $\langle \mathcal{S}, \mathcal{A}, P, r \rangle$, where $\mathcal{S} \subseteq \mathbb{R}^{d_S}$ and $\mathcal{A} \subseteq \mathbb{R}^{d_A}$ are continuous state and action spaces, respectively; $P : \mathcal{S} \times \mathcal{A} \rightarrow (\mathcal{S} \rightarrow [0, 1])$ represents the transition probability kernel, and $r : \mathcal{S} \times \mathcal{A} \rightarrow \mathbb{R}$ is the reward function. Moreover, we make a smoothness assumption on P ,

Assumption 1. *The transition probability kernel P is Lipschitz w.r.t. its action variable, in the sense that there exists $C > 0$ such that for all $(s, a, a') \in \mathcal{S} \times \mathcal{A} \times \mathcal{A}$ and measurable set $\mathcal{B} \subset \mathcal{S}$,*

$$|P(\mathcal{B}|s, a) - P(\mathcal{B}|s, a')| \leq C\|a - a'\|. \quad (1)$$

Assumption 1 has been used in the literature for learning in domains with continuous state-action spaces [10], as the assumption on the smoothness of MDP becomes crucial in such environments [10, 11, 12]. Note that we only use the Lipschitz smoothness assumption on P for the theoretical convenience, and we later provide experimental results in environments that do not satisfy this assumption. Furthermore, we assume that the state and action spaces are inner product spaces.

We present the trajectory of selected actions in the action space \mathcal{A} with $\tau_{\mathcal{A}} = (a_0, \dots, a_{T-1})$ and the trajectory of the visited states in the state space \mathcal{S} with $\tau_{\mathcal{S}} = (s_0, \dots, s_{T-1})$. Moreover, we define

$$\Omega(\tau_{\mathcal{S}}, \tau_{\mathcal{A}}) := \{s \in \mathcal{S} \mid \Pr[S_T = s \mid s_{T-1}, a_{T-1}] > 0\} \quad (2)$$

as the set of probable states $s \in \mathcal{S}$ observed at time T given s_{T-1} from $\tau_{\mathcal{S}}$ and the selected action a_{T-1} from $\tau_{\mathcal{A}}$. Note that T is the number of time steps since the start of the respective piece-wise exploratory trajectory, and is reset at each exploitation step. For simplicity, in the rest of this manuscript, we denote $\Omega(\tau_{\mathcal{S}}, \tau_{\mathcal{A}})$ by Ω . In addition, the concatenation of the trajectory $\tau_{\mathcal{S}}$ and the state s visited at time step T is denoted as the trajectory $\tau'_{\mathcal{S}} := (\tau_{\mathcal{S}}, s)$. Moreover, for the theoretical analysis purposes, and in order to show the expansion of the visited-states trajectory in the state space, we choose to transform $\tau_{\mathcal{S}}$ into a sequence of vectors connecting every two consecutive states (bond vectors),

$$\omega_{\tau_{\mathcal{S}}} = \{\omega_i\}_{i=1}^{T-1}, \quad \text{where } \omega_i = s_i - s_{i-1}. \quad (3)$$

Finally, we define Self-Avoiding Random Walks (LSA-RWs), inspired by the theory of freely-rotating chains (FRCs), where the correlation between $|i - j|$ consecutive bond vectors is a decaying exponential with the correlation number L_p (persistence number). L_p represents the number of time steps, after which the bond vectors forget their initial orientation.

Definition 1 (Locally Self-Avoiding Random Walks (LSA-RWs)). *A sequence of random bond vectors $\omega = \{\omega_i\}_{i=1}^T$ is Locally Self-Avoiding with persistence number $L_p > 1$, if for all $i, j \in [T]$ there exists $b_o > 0$ such that, (1)*

$\langle \|w_i\|^2 \rangle = b_o^2$ and 2) $\langle w_i \cdot w_j \rangle \sim b_o^2 e^{\frac{-|j-i|}{L_p}}$, where $\langle \cdot \rangle$ denotes the ensemble average over all configurations of the chain induced by the dynamic randomness of the environment (equivalent to the thermal fluctuations in the environment in statistical physics).

The first condition states that the expected magnitude of each bond vector is b_o . The second condition shows that the correlation between $|i - j|$ consecutive bond vectors is a decaying exponential with the correlation length L_p (persistence number), which is the number of time steps after which the bond vectors forget their original orientation. Note that despite the redundancy of the first condition, we choose to include it separately in order to emphasize the finite expected magnitude of the bond vectors.

3 Methods

We introduce the method of polymer-based exploration in reinforcement learning (PolyRL), which borrows concepts from Statistical Physics [13, 14] to induce persistent trajectories in continuous state-action spaces (Refer to the Appendix (Section A) for more information regarding polymer models). As discussed below, our proposed technique balances exploration and exploitation using high-probability confidence bounds on a measure of spread in the state space. Algorithm 1 presents the PolyRL pseudo code. The method of action sampling is provided in the Appendix (Section C).

Algorithm 1 PolyRL Algorithm

Require: Exploration factor β , Average correlation angle θ and Correlation variance σ^2

for N in total number of episodes **do**

$\delta \leftarrow 1 - e^{-\beta N}$ ▷ An increasing function of the the episode number.

Sample \mathbf{a}_0 and \mathbf{s}_0 from an initial state-action distribution, and Exploit-flag $\leftarrow 0$

repeat

if Exploit-flag == 1 **then**

Draw a random number $\kappa \sim \mathcal{N}(0, 1)$

if $\kappa \leq \delta$ **then**

$\mathbf{a}_t \sim \pi_\mu$ ▷ action is drawn from the target policy

else

Exploit-flag $\leftarrow 0$

Start a new exploratory trajectory by setting the radius of gyration squared to zero

Draw random number $\eta \sim \mathcal{N}(\theta, \sigma^2)$

$\mathbf{a}_t \sim \pi_{\text{PolyRL}}(\eta, \mathbf{a}_{t-1})$

end if

else

Compute the change in the radius of gyration squared ΔU_g^2 letting $d = L_2$ -norm and using eq. (4).

Calculate UB and LB using eqs. (7) and (11).

if $\Delta U_g^2 \geq LB$ and $\Delta U_g^2 \leq UB$ **then**

Draw random number $\eta \sim \mathcal{N}(\theta, \sigma^2)$

$\mathbf{a}_t \sim \pi_{\text{PolyRL}}(\eta, \mathbf{a}_{t-1})$

else

Exploit-flag $\leftarrow 1$, and $\mathbf{a}_t \sim \pi_\mu$

end if

end if

until reaching an absorbing state or the maximum allowed time steps in an episode

end for

The PolyRL agent chooses the sequence of actions in \mathcal{A} such that every two consecutive action vectors are restricted in their orientation with the mean [correlation] angle θ . In order to induce persistent trajectories in the state space, the agent uses a measure of spread in the visited states in order to ensure the desired expansion of the trajectory τ_S in \mathcal{S} . We define *radius of gyration squared*,

$$U_g^2(\tau_S) := \frac{1}{T-1} \sum_{s \in \tau_S} d^2(s, \bar{\tau}_S), \quad (4)$$

as a measure of the spread of the visited states in the state space \mathcal{S} , where $d(s, \bar{\tau}_S)$ is a metric defined on the state space \mathcal{S} , and serves as a measure of distance between a visited state s and the empirical mean of all visited states $\bar{\tau}_S$. Also known as the center of mass, $\bar{\tau}_S$ is calculated as, $\bar{\tau}_S := \frac{1}{T} \sum_{s \in \tau_S} s$.

At each time step, the agent calculates the radius of gyration squared (equation 4) and compares it with the obtained value from the previous time step. If the induced trajectory in the state space is LSA-RW, it maintains an expected stiffness described by a bounded change in U_g^2 . Theorems 3 and 4 show high-probability confidence bounds on upper local sensitivity UB and lower local sensitivity LB , respectively. The lower bound ensures that the chain remains LSA-RW and expands in the space, while the upper bound prevents the agent from moving abruptly in the environment (The advantage of using LSA-RWs to explore the environment can be explained in terms of their high expansion rate, which is presented in Proposition 7 in the Appendix). If the computed ΔU_g^2 is in the range $[LB, UB]$, the agent continues to perform PolyRL action sampling method (Algorithm 2 in the Appendix). Otherwise, it samples the next action using the target policy. The factor $\delta \in [0, 1]$ that arises in equations 7 and 11 controls the tightness of the confidence interval. In order to balance the trade-off between exploration and exploitation, we choose to increase δ with time, as increasing δ leads to tighter bounds and thus higher probability of exploitation. In addition, the exploration factor δ determines the probability of switching from exploitation back to starting a new exploratory trajectory. Due to the persistence of the PolyRL chain of exploratory actions, the orientation of the last greedy action is preserved for Lp (persistence) number of steps. As for the trajectories in the state space, upon observing correlation angles above $\pi/2$, the exploratory trajectory is broken and the next action is chosen with respect to the target policy π_μ .

4 Related Work

A wide range of exploration techniques with theoretical guarantees (*e.g.* PAC bounds) have been developed for MDPs with finite or infinitely countable state or action spaces [15, 16, 17, 18, 19, 20, 21], however extending these algorithms to real-world settings with continuous state and action spaces without any assumption on the structure of state-action spaces or the reward function is impractical [22, 23].

Perturbation-based exploration strategies are, by nature, agnostic to the structure of the underlying state-action spaces and are thus suitable for continuous domains. Classic perturbation-based exploration strategies typically involve a perturbation mechanism at either the action-space or the policy parameter-space level. These methods subsequently employ stochasticity at the policy level as the main driving force for exploration [24]. Methods that apply perturbation at the parameter level often preserve the noise distribution throughout the trajectory [12, 25, 26, 27, 28, 29], and do not utilize the trajectory information in this regard. Furthermore, a majority of action-space perturbation approaches employ per-step independent or correlated perturbation [30, 31, 22, 32]. For instance, [31] uses the Ornstein–Uhlenbeck (OU) process to produce auto-correlated additive noise at the action level and thus benefit from the correlated noise between consecutive actions.

While maintaining correlation between consecutive actions is advantageous in many locomotion tasks [33, 34, 35], it brings technical challenges due to the non-Markovian nature of the induced decision process [36], which leads to substantial dependence on the history of the visited states. This challenge is partially resolved in the methods that benefit from some form of parametric memory (*e.g.* OU processes) [29, 31]. However, they all suffer from the lack of *informed orientational persistence*, *i.e.* the agent’s persistence in selecting actions that preserve the orientation of the state trajectory induced by the target policy. Particularly in sparse-reward structured environments, where the agent rarely receives informative signals, the agent will eventually get stuck in a small region since the analytical change on the gradient of greedy policy is minimal [37, 38]. Hence, the agent’s persistent behaviour in action sampling with respect to the local history (short-term memory) of the selected state-action pairs plays a prominent role in exploring the environments with sparse or delayed reward structures.

5 Theory

In this section, we derive the upper and lower confidence bounds on the local sensitivity for the radius of gyration squared between τ_S and τ'_S (All proofs are provided in the Appendix (Section B)). Given the trajectory τ_S and the corresponding radius of gyration squared $U_g^2(\tau_S)$ and persistence number $Lp_{\tau_S} > 1$, we seek a description for the permissible range of $U_g^2(\tau'_S)$ such that the stiffness of the trajectory is preserved.

High-probability upper bound - We define the upper local sensitivity on U_g^2 upon observing new state $s_T \in \mathcal{S}$ as,

$$ULS_{U_g^2}(\tau_S) := \sup_{s_T \in \Omega} U_g^2(\tau'_S) - U_g^2(\tau_S). \quad (5)$$

Given the observed state trajectory τ_S with persistence number Lp_{τ_S} , the upper local sensitivity $ULS_{U_g^2}$ provides the maximum change observed upon visiting the next accessible state $s' \in \Omega$. With the goal of constructing the new trajectory τ'_S such that it preserves the stiffness induced by τ_S , we calculate the high-probability upper confidence bound on $ULS_{U_g^2}$. To do so, we write the term $d^2(s, \bar{\tau}_S)$ in equation 4 as a function of bond vectors ω_i , which is presented in lemma 2 given that $d = L_2$ -norm. We further substitute the resulting $U_g^2(\tau_S)$ in equation 5 with the obtained expression from equation 4.

Lemma 2. Let $\tau_S = (s_0, \dots, s_{T-1})$ be the trajectory of visited states, s_T be a newly visited state and $\omega_i = s_i - s_{i-1}$ be the bond vector that connects two consecutive visited states s_{i-1} and s_i . Then we have,

$$\|s_T - \bar{\tau}_S\|^2 = \|\omega_T + \frac{1}{T} \left[\sum_{i=1}^{T-1} i\omega_i \right]\|^2. \quad (6)$$

The result of lemma 2 will be used in the proof of theorem 3, as shown in the Appendix (Section B.2). In theorem 3 below, we provide a high-probability upper bound for $ULS_{Ug^2}(\tau_S)$.

Theorem 3 (Upper-Bound Theorem). Let $\delta \in (0, 1)$ and τ_S be a LSA-RW in \mathcal{S} induced by PolyRL with the persistence number $Lp_{\tau_S} > 1$ within episode N , $\omega_{\tau_S} = \{\omega_i\}_{i=1}^{T-1}$ be the sequence of corresponding bond vectors, where $T > 0$ denotes the number of bond vectors within τ_S , and b_o be the average bond length. The upper confidence bound for $ULS_{Ug^2}(\tau_S)$ with probability of at least $1 - \delta$ is,

$$UB = \Lambda(T, \tau_S) + \frac{1}{\delta} \left[\Gamma(T, b_o, \tau_S) + \frac{2b_o^2}{T^2} \sum_{i=1}^{T-1} i e^{\frac{-(T-i)}{Lp_{\tau_S}}} \right], \quad (7)$$

where,

$$\Lambda(T, \tau_S) = -\frac{1}{T-1} U_g^2(\tau_S) \quad (8)$$

$$\Gamma(T, b_o, \tau_S) = \frac{b_o^2}{T} + \frac{\|\sum_{i=1}^{T-1} i\omega_i\|^2}{T^3} \quad (9)$$

Equation 7 provides an upper bound on the pace of the trajectory expansion in the state space, and thus prevents the agent from moving abruptly in the environment, which would lead to a break in its temporal correlation with the preceding states. Similarly, we introduce the lower local sensitivity LLS_{Ug^2} , which provides the minimum change observed upon visiting the next accessible state $s' \in \Omega$.

High-probability lower bound - In this section, We define the lower local sensitivity on U_g^2 upon observing new state $s_T \in \mathcal{S}$ as,

$$LLS_{Ug^2}(\tau_S) := \inf_{s_T \in \Omega} U_g^2(\tau'_S) - U_g^2(\tau_S). \quad (10)$$

We further compute the high-probability lower confidence bound on LLS_{Ug^2} in order to guarantee the expansion of the trajectory τ_S upon visiting the next state.

Theorem 4 (Lower-Bound Theorem). Let $\delta \in (0, 1)$ and τ_S be a LSA-RW in \mathcal{S} induced by PolyRL with the persistence number $Lp_{\tau_S} > 1$ within episode N , $\omega_{\tau_S} = \{\omega_i\}_{i=1}^{T-1}$ be the sequence of corresponding bond vectors, where $T > 0$ denotes the number of bond vectors within τ_S , and b_o be the average bond length. The lower confidence bound for $LLS_{Ug^2}(\tau_S)$ at least with probability $1 - \delta$ is,

$$LB = \Lambda(T, \tau_S) + (1 - \sqrt{2 - 2\delta}) \times \left[\Gamma(T, b_o, \tau_S) + \frac{(T-1)(T-2)}{T^2} b_o^2 e^{\frac{-|T-1|}{Lp_{\tau_S}}} \right], \quad (11)$$

where,

$$\Lambda(T, \tau_S) = -\frac{1}{T-1} U_g^2(\tau_S) \quad (12)$$

$$\Gamma(T, b_o, \tau_S) = \frac{b_o^2}{T} + \frac{\|\sum_{i=1}^{T-1} i\omega_i\|^2}{T^3} \quad (13)$$

Equation 11 provides a lower bound on the change in the expansion of the trajectory. Note that for the experimental purposes, we let $\delta = 1 - e^{-\beta N}$, where the exploration factor $\beta \in (0, 1)$ is a hyper parameter and N is the number of elapsed episodes.

The following corollary is an immediate consequence of theorems 3 and 4 together with Assumption 1.

Corollary 5. Given that assumption 1 in the manuscript is satisfied, with high probability the exploratory trajectories formed in \mathcal{S} induced by PolyRL Algorithm are LSA-RWs.

The proof is provided and discussed thoroughly in the Appendix (Section B.4).

6 Experiments

As an exploration method, PolyRL should be assessed in comparison with other exploration techniques, and thus must accompany an off-policy learning method to generate data for. In this section, we integrate PolyRL with three learning algorithms: (1) the Q-learning method ([39]) with linear function approximation in a 2D sparse continuous state-and-action navigation task, where the performance of PolyRL is compared with that of ϵ -greedy; (2) the deep deterministic policy gradients (DDPG) [31] algorithm, where PolyRL (DDPG-PolyRL) is assessed in comparison with additive uncorrelated Gaussian action space noise (DDPG-UC), correlated Ornstein-Uhlenbeck action space noise (DDPG-OU) [40, 31], as well as adaptive parameter space noise (DDPG-PARAM) [41]; and (3) the Soft Actor-Critic (SAC) algorithm [42], where PolyRL is combined with SAC (SAC-PolyRL) and replaces the random exploration phase during the first 10,000 steps in the SAC algorithm. The sets of experiments with the learning methods DDPG and SAC are performed in MuJoCo high-dimensional continuous control tasks “SparseHopper-V2” ($\mathcal{A} \subset \mathbb{R}^3$, $\mathcal{S} \subset \mathbb{R}^{11}$), “SparseHalfCheetah-V2” ($\mathcal{A} \subset \mathbb{R}^6$, $\mathcal{S} \subset \mathbb{R}^{17}$), and “SparseAnt-V2” ($\mathcal{A} \subset \mathbb{R}^8$, $\mathcal{S} \subset \mathbb{R}^{11}$) (Refer to the Appendix (Section D) for the bench-marking results of the same algorithms in the standard (dense-reward) MuJoCo tasks.).

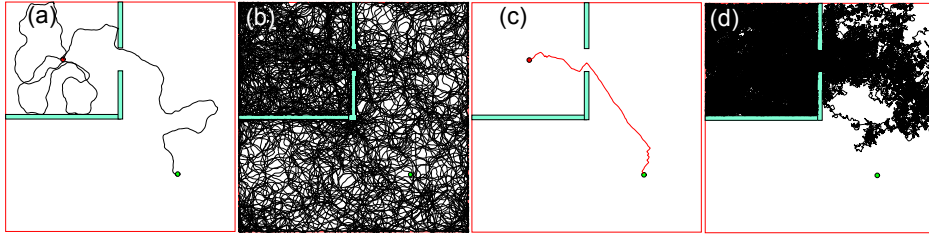


Figure 1: Visualization of the agent’s trajectory in a 2D navigation task with continuous state-action space and sparse-reward structure. The environment is composed of a 100×100 big chamber and a 50×50 smaller chamber. The start state is located inside the small chamber (the red circle with a diameter of 1), and the goal is outside the small chamber (the green circle with a diameter of 1). The agent receives +100 reward when it reaches the goal and 0 reward elsewhere. (a-c) Performance of the PolyRL agent with the correlation angle $\theta \simeq 0.2$. (a) A sample trajectory of the PolyRL agent in one episode. (b) Coverage of the environment after 11 episodes. (c) A sample trajectory of the PolyRL agent during the evaluation phase after learning the task. (d) The ϵ -greedy agent’s coverage of the environment after 11 episodes.

Algorithm and Environment Settings - The environment in our 2D sparse-reward navigation tasks either consists of only one 400×400 chamber (goal reward +1000), or a 50×50 room encapsulated by a 100×100 chamber. Initially positioned inside the small room, the agent’s goal in the latter case is to find its way towards the bigger chamber, where the goal is located (goal reward +100) (Figure 1). Moreover, in order to make the former task more challenging, in a few experiments, we introduce a *puddle* in the environment, where upon visiting, the agent receives the reward -100 . In order to assess the agent’s performance, we integrate the PolyRL exploration algorithm with the Q-learning method with linear function approximation (learning rate = 0.01) and compare the obtained results with those of the ϵ -greedy exploration with Q-learning. We subsequently plot the quantitative results for the former task and visualize the resulting trajectories for the latter.

In the sparse MuJoCo tasks, the agent receives a reward of +1 only when it crosses a target distance λ , termed the *sparsity threshold*. Different λ values can change the level of difficulty of the tasks significantly. Note that due to the higher performance of SAC compared with that of DDPG, we have elevated λ for SAC-based experiments, making the tasks more challenging. Moreover, we perform an exhaustive grid search over the corresponding hyper parameters for each task. The sparsity thresholds, the obtained hyper-parameter values, as well as the network architecture of the learning algorithms DDPG and SAC are provided in the Appendix (Section E).

Results and Discussion - We present the qualitative results for the 2D sparse navigation task in figure 1. An example of PolyRL trajectory in one episode (figure 1 (a)) demonstrates the expansion of the PolyRL agent trajectory in the environment. After 11 episodes, the PolyRL agent exhibits a full coverage of the environment (figure 1 (b)) and is consequently able to learn the task (figure 1 (c)), while the ϵ -greedy agent is not able to reach the goal state even once, and thus fails to learn the task (figure 1 (d)). This visual observation highlights the importance of space coverage in sparse-reward tasks, where the agent rarely receives informative reinforcement from the environment. An effective trajectory expansion in the environment exposes the agent to the unvisited regions of the space. It thus increases the frequency of receiving informative reinforcement and accelerates the learning process. In Fig. 2, the quantitative results for learning the task in a similar environment (the 400×400 chamber) are shown both in the absence (figure 2 (a)) and

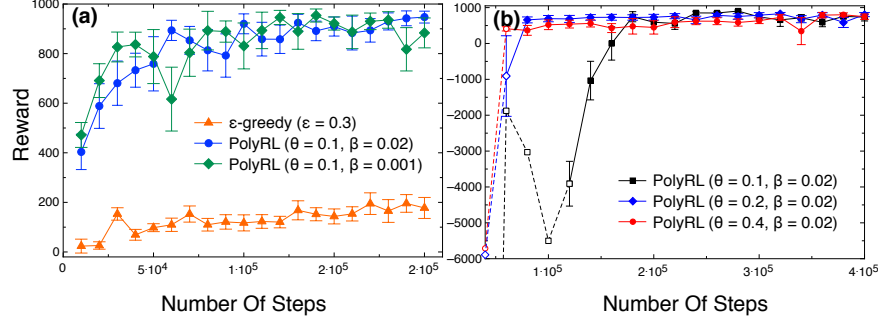


Figure 2: The performance of PolyRL and ϵ -greedy in a 2D continuous sparse-reward navigation task (the 400×400 chamber). (a) The environment does not include a puddle. (b) The environment contains a puddle. The first point on the $\theta = 0.1$ curve is not shown on the graph due to its minimal average reward value ($\simeq -30000$), which affects the range of the y-axis. It is connected to the next point via a dashed line. The data points on the dashed lines do not include error bars because of substantial variances. For the same reason (out of range values and large variances), the results for the ϵ -greedy exploration method are not shown here.

presence (figure 2 (b)) of a puddle. In both cases, the PolyRL exploration method outperforms ϵ -greedy significantly. In figure 2 (b), we observe that trajectories with lower persistence (larger θ) present a better performance compared with stiffer trajectories. Note that due to the existence of walls in these 2D tasks, the transition probability kernel is specifically non-smooth at the walls. Thus, the smoothness assumption on the transition probability kernel made earlier for the theoretical convenience does not apply in these specific environments. Yet, we empirically show that PolyRL still achieves a high performance in learning these tasks.

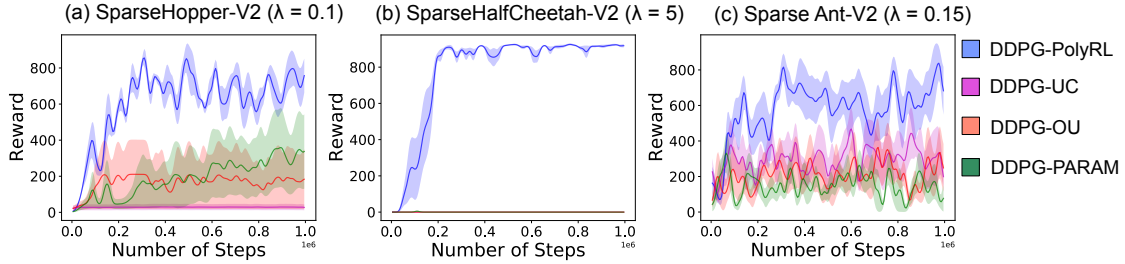


Figure 3: The simulation results for DDPG-based methods in “SparseHopper-v2” (a), “SparseHalfCheetah-v2” (b) and “SparseAnt-v2” (c). The sparsity thresholds for these tasks are $\lambda = 0.1$, $\lambda = 5$, and $\lambda = 0.15$, respectively. The results are averaged over 5 random seeds. The error bars depict the standard error on the mean (Refer to the Appendix (Section D) for the results of the baseline algorithms).

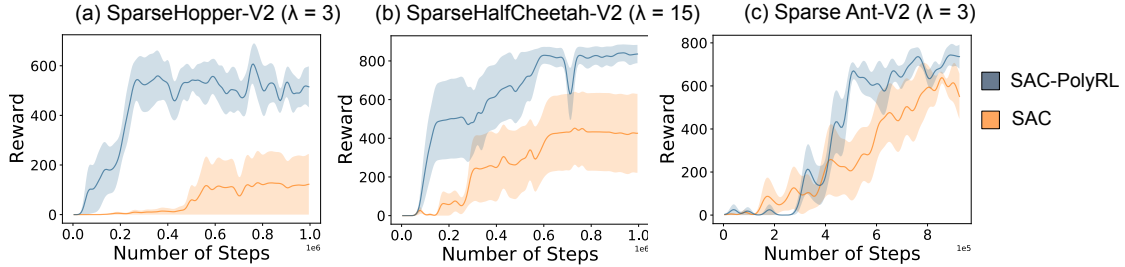


Figure 4: The simulation results for SAC and SAC-PolyRL in “SparseHopper-v2” (a), “SparseHalfCheetah-v2” (b) and “SparseAnt-v2” (c). The sparsity thresholds for these tasks are $\lambda = 3$, $\lambda = 15$, and $\lambda = 3$, respectively. The results are averaged over 5 random seeds. The error bars depict the standard error on the mean (Refer to the Appendix (Section D) for the results of the baseline algorithms).

We illustrate the results in sparse MuJoCo tasks for DDPG-based and SAC-based methods in figures 3 and 4, respectively. The obtained results in SparseHopper-V2, SparseHalfCheetah-V2, and SparseAnt-V2 show that integrating the two learning methods (SAC and DDPG) with the exploration algorithm PolyRL leads to improvement in the learning performance. The remarkable results achieved by the PolyRL exploration method confirms that the agent has been able to efficiently and sufficiently cover the space, receive informative reinforcement, and learn the tasks. The high performance of SAC-PolyRL (figure 4) is particularly significant, in the sense that PolyRL assists SAC in the data generation process only for the first 10,000 steps, after which SAC fills in and continues with the learning process. Yet, this short presence leads to a notable contribution in enhancing the performance of SAC.

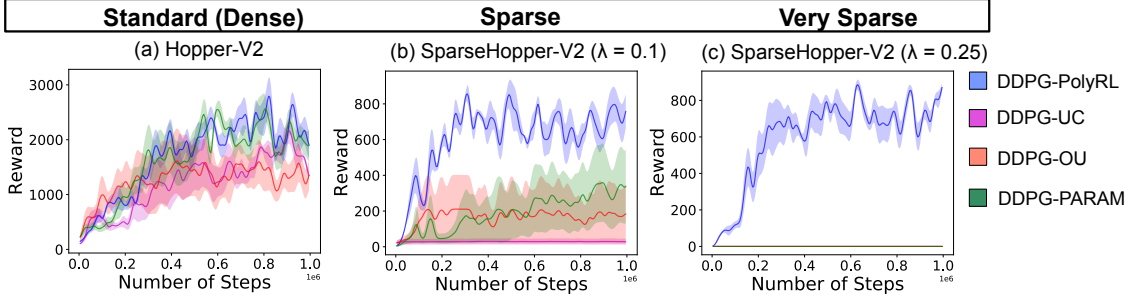


Figure 5: DDPG-PolyRL sensitivity to the change of sparsity threshold. The experimental results are presented in standard (dense reward) “Hopper-v2” (a), “SparseHopper-v2” for sparsity threshold $\lambda = 0.1$ (b), and “SparseHopper-v2” for sparsity threshold $\lambda = 0.25$ (c).

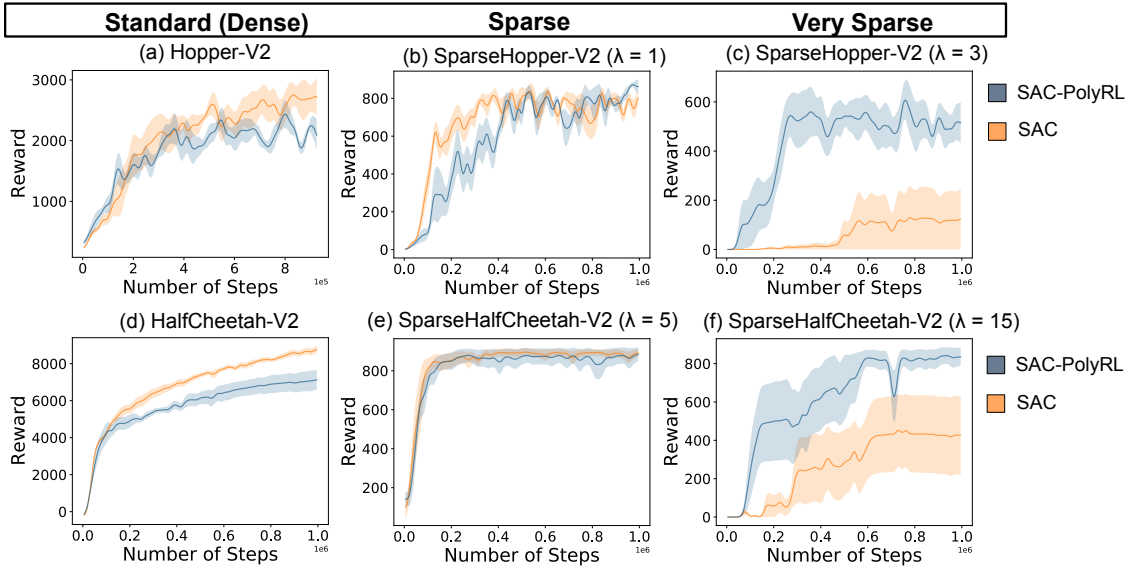


Figure 6: SAC-PolyRL sensitivity to the change of sparsity threshold in sample experiments. The column on the left depicts the results for standard (dense reward) MuJoCo tasks. From left to right, the sparsity of the reward structure increases.

A notable feature of PolyRL is its relatively low sensitivity to the increase in sparsity threshold λ compared to that of other DDPG-based and SAC algorithms. The performance of PolyRL combined with DDPG (Figure 5) and SAC (Figure 6) is illustrated in tasks for three different sparsity thresholds. The level of complexity of the tasks increases from left to right with the sparsity threshold λ . As the sparsity level changes from sparse to very sparse, the graphs demonstrate a sharp decrease in the performance of PolyRL counterparts, while the PolyRL performance stays relatively stable (Note that due to the reward structure in these sparse tasks and considering that the maximum number of steps in each episode is by default set to 1000 in the gym environments, the maximum reward that an agent could get during each evaluation round cannot exceed 1000). This PolyRL agent’s behaviour can be explained by its relatively fast expansion in the space (Refer to Proposition 7 in the Appendix), which leads to faster access to the sparsely distributed

rewards compared with other DDPG-based and SAC methods. On the other hand, PolyRL does not perform as well in standard tasks, where the reinforcement is accessible to the agents at each time-step. Since PolyRL does not use the received rewards in its action selection process, it does not behave targeted. Thus, in the environments with dense reward structures, PolyRL might skip the informative signals nearby and move on to the farther regions in the space, leading to acquiring less amount of information and lower performance. In other words, the strength of PolyRL is most observable in the tasks where accessing information is limited or delayed.

7 Conclusion

We propose a new exploration method in reinforcement learning (PolyRL), which leverages the notion of locally self-avoiding random walks and is designed for environments with continuous state-action spaces and sparse-reward structures. The most interesting aspect of our proposal is the explicit construction of each exploratory move based on the entire existing trajectory, rather than just the current observed state. While the agent chooses its next move based on its current state, the inherent locally self-avoiding property of the walk acts as an implicit memory, which governs the agent’s exploratory behaviour. Yet this locally controlled behavior leads to an interesting global property for the trajectory, which is an improvement in the coverage of the environment. This feature, as well as not relying on extrinsic rewards in the decision-making process, makes PolyRL perfect for the sparse-reward tasks. We assess the performance of PolyRL in 2D continuous sparse navigation tasks, as well as three sparse high-dimensional simulation tasks, and show that PolyRL performs significantly better than the other exploration methods in combination with the baseline algorithms DDPG and SAC. Finally, a more adaptive version of PolyRL, which can map the changes in the action trajectory stiffness to that of the state trajectory, could be helpful in more efficient learning of the simulation tasks.

8 Acknowledgements

The authors would like to thank Prof. Walter Reisner for providing valuable feedback on the initial direction of this work, and Riashat Islam for helping with the experiments in the early stages of the project. Computing resources were provided by Compute Canada and Calcul Québec throughout the project, and by Deeplite Company for preliminary data acquisition, which the authors appreciate.

References

- [1] Justin Fu, John Co-Reyes, and Sergey Levine. Ex2: Exploration with exemplar models for deep reinforcement learning. In *Advances in neural information processing systems*, pages 2577–2587, 2017.
- [2] Ashvin Nair, Bob McGrew, Marcin Andrychowicz, Wojciech Zaremba, and Pieter Abbeel. Overcoming exploration in reinforcement learning with demonstrations. In *2018 IEEE International Conference on Robotics and Automation (ICRA)*, pages 6292–6299. IEEE, 2018.
- [3] Marcin Andrychowicz, Filip Wolski, Alex Ray, Jonas Schneider, Rachel Fong, Peter Welinder, Bob McGrew, Josh Tobin, OpenAI Pieter Abbeel, and Wojciech Zaremba. Hindsight experience replay. In I. Guyon, U. V. Luxburg, S. Bengio, H. Wallach, R. Fergus, S. Vishwanathan, and R. Garnett, editors, *Advances in Neural Information Processing Systems 30*, pages 5048–5058. Curran Associates, Inc., 2017.
- [4] Adrien Ali Taïga, William Fedus, Marlos C Machado, Aaron Courville, and Marc G Bellemare. Benchmarking bonus-based exploration methods on the arcade learning environment. *arXiv preprint arXiv:1908.02388*, 2019.
- [5] Georg Ostrovski, Marc G Bellemare, Aäron van den Oord, and Rémi Munos. Count-based exploration with neural density models. In *Proceedings of the 34th International Conference on Machine Learning-Volume 70*, pages 2721–2730. JMLR. org, 2017.
- [6] Rein Houthooft, Xi Chen, Yan Duan, John Schulman, Filip De Turck, and Pieter Abbeel. Vime: Variational information maximizing exploration. In *Advances in Neural Information Processing Systems*, pages 1109–1117, 2016.
- [7] Kamil Ciosek, Quan Vuong, Robert Loftin, and Katja Hofmann. Better exploration with optimistic actor critic. In *Advances in Neural Information Processing Systems*, pages 1785–1796, 2019.
- [8] Will Dabney, Georg Ostrovski, and André Barreto. Temporally-extended $\{\epsilon\}$ -greedy exploration. *arXiv preprint arXiv:2006.01782*, 2020.
- [9] Aravind S Lakshminarayanan, Sahil Sharma, and Balaraman Ravindran. Dynamic action repetition for deep reinforcement learning. In *Proceedings of the Thirty-First AAAI Conference on Artificial Intelligence*, pages 2133–2139, 2017.

- [10] András Antos, Csaba Szepesvári, and Rémi Munos. Fitted q-iteration in continuous action-space mdps. In *Advances in neural information processing systems*, pages 9–16, 2008.
- [11] Peter L Bartlett and Ambuj Tewari. Sample complexity of policy search with known dynamics. In *Advances in Neural Information Processing Systems*, pages 97–104, 2007.
- [12] Andrew Y Ng and Michael Jordan. Pegasus: a policy search method for large mdps and pomdps. In *Proceedings of the Sixteenth conference on Uncertainty in artificial intelligence*, pages 406–415, 2000.
- [13] Pierre-Giles de Gennes. *Scaling concepts in polymer physics*. Cornel University Press, 1979.
- [14] Masao Doi and Samuel Frederick Edwards. *The theory of polymer dynamics*, volume 73. oxford university press, 1988.
- [15] Michael Kearns and Satinder Singh. Near-optimal reinforcement learning in polynomial time. *Machine Learning*, 49(2-3):209–232, 2002.
- [16] Ronen I Brafman and Moshe Tennenholtz. R-max-a general polynomial time algorithm for near-optimal reinforcement learning. *Journal of Machine Learning Research*, 3(Oct):213–231, 2002.
- [17] A Strehl and M Littman. Exploration via model based interval estimation. In *International Conference on Machine Learning*. Citeseer, 2004.
- [18] Manuel Lopes, Tobias Lang, Marc Toussaint, and Pierre-Yves Oudeyer. Exploration in model-based reinforcement learning by empirically estimating learning progress. In *Advances in Neural Information Processing Systems*, pages 206–214, 2012.
- [19] Mohammad Gheshlaghi Azar, Ian Osband, and Rémi Munos. Minimax regret bounds for reinforcement learning. In *Proceedings of the 34th International Conference on Machine Learning-Volume 70*, pages 263–272. JMLR.org, 2017.
- [20] Martha White and Adam White. Interval estimation for reinforcement-learning algorithms in continuous-state domains. In *Advances in Neural Information Processing Systems*, pages 2433–2441, 2010.
- [21] Yuanhao Wang, Kefan Dong, Xiaoyu Chen, and Liwei Wang. Q-learning with ucb exploration is sample efficient for infinite-horizon mdp. In *International Conference on Learning Representations*, 2020.
- [22] T. Haarnoja, H. Tang, P. Abbeel, and S. Levine. Reinforcement learning with deep energy-based policies. In *Proceedings of the International Conference on Machine Learning*, 2017.
- [23] Rein Houthooft, Xi Chen, Xi Chen, Yan Duan, John Schulman, Filip De Turck, and Pieter Abbeel. VIME: variational information maximizing exploration. In *Advances in Neural Information Processing Systems 29: Annual Conference on Neural Information Processing Systems 2016, December 5-10, 2016, Barcelona, Spain*, pages 1109–1117, 2016.
- [24] Marc Peter Deisenroth, Gerhard Neumann, Jan Peters, et al. A survey on policy search for robotics. *Foundations and Trends® in Robotics*, 2(1–2):1–142, 2013.
- [25] Frank Sehnke, Christian Osendorfer, Thomas Rückstieß, Alex Graves, Jan Peters, and Jürgen Schmidhuber. Parameter-exploring policy gradients. *Neural Networks*, 23(4):551–559, 2010.
- [26] Evangelos Theodorou, Jonas Buchli, and Stefan Schaal. A generalized path integral control approach to reinforcement learning. *Journal of Machine Learning Research*, 11(Nov):3137–3181, 2010.
- [27] Meire Fortunato, Mohammad Gheshlaghi Azar, Bilal Piot, Jacob Menick, Ian Osband, Alex Graves, Vlad Mnih, Remi Munos, Demis Hassabis, Olivier Pietquin, et al. Noisy networks for exploration. *arXiv preprint arXiv:1706.10295*, 2017.
- [28] Cédric Colas, Olivier Sigaud, and Pierre-Yves Oudeyer. GEP-PG: Decoupling exploration and exploitation in deep reinforcement learning algorithms. In *Proceedings of the 35th International Conference on Machine Learning*, volume 80 of *Proceedings of Machine Learning Research*, pages 1039–1048, 2018.
- [29] Matthias Plappert, Rein Houthooft, Prafulla Dhariwal, Szymon Sidor, Richard Y. Chen, Xi Chen, Tamim Asfour, Pieter Abbeel, and Marcin Andrychowicz. Parameter space noise for exploration. In *International Conference on Learning Representations*, 2018.
- [30] Paweł Wawrzyński. Real-time reinforcement learning by sequential actor-critics and experience replay. *Neural Networks*, 22(10):1484–1497, 2009.
- [31] Timothy P Lillicrap, Jonathan J Hunt, Alexander Pritzel, Nicolas Heess, Tom Erez, Yuval Tassa, David Silver, and Daan Wierstra. Continuous control with deep reinforcement learning. *arXiv preprint arXiv:1509.02971*, 2015.
- [32] Tianbing Xu, Qiang Liu, Liang Zhao, and Jian Peng. Learning to explore with meta-policy gradient. In *Proceedings of the International Conference on Machine Learning*, volume 80, pages 5459–5468, 2018.

- [33] Jun Morimoto and Kenji Doya. Acquisition of stand-up behavior by a real robot using hierarchical reinforcement learning. *Robotics and Autonomous Systems*, 36(1):37–51, 2001.
- [34] Jens Kober, J Andrew Bagnell, and Jan Peters. Reinforcement learning in robotics: A survey. *The International Journal of Robotics Research*, 32(11):1238–1274, 2013.
- [35] Abhishek Gupta, Russell Mendonca, YuXuan Liu, Pieter Abbeel, and Sergey Levine. Meta-reinforcement learning of structured exploration strategies. In *Advances in Neural Information Processing Systems*, pages 5302–5311, 2018.
- [36] Julien Perez and Tomi Silander. Non-markovian control with gated end-to-end memory policy networks. *arXiv preprint arXiv:1705.10993*, 2017.
- [37] Joshua Hare. Dealing with sparse rewards in reinforcement learning. *arXiv preprint arXiv:1910.09281*, 2019.
- [38] Bingyi Kang, Zequn Jie, and Jiashi Feng. Policy optimization with demonstrations. In *International Conference on Machine Learning*, pages 2469–2478, 2018.
- [39] Christopher JCH Watkins and Peter Dayan. Q-learning. *Machine learning*, 8(3-4):279–292, 1992.
- [40] George E Uhlenbeck and Leonard S Ornstein. On the theory of the brownian motion. *Physical review*, 36(5):823, 1930.
- [41] Matthias Plappert, Rein Houthooft, Prafulla Dhariwal, Szymon Sidor, Richard Y Chen, Xi Chen, and others. Parameter space noise for exploration. *arXiv preprint arXiv:1706.01905*, 2017.
- [42] Tuomas Haarnoja, Aurick Zhou, Pieter Abbeel, and Sergey Levine. Soft actor-critic: Off-policy maximum entropy deep reinforcement learning with a stochastic actor. In *International Conference on Machine Learning*, pages 1861–1870, 2018.
- [43] M Rubenstein and RH Colby. Polymer physics: Oxford university press, 2003.

Appendix

Here, we provide additional information on different parts of the paper. In particular, in section A we introduce and discuss two chain models in polymer physics. In section B, we provide the theoretical proofs of theorems 3 and 4, lemma 2, and corollary 5 in the manuscript. In section C, we present the action-sampling algorithm, and in section D we provide some additional baseline results in the standard MuJoCo tasks. Finally, in section E, we provide the network architecture of the learning methods, as well as the PolyRL hyper parameters used in the experimental section.

A Polymer Models

In the field of *Polymer Physics*, the conformations and interactions of polymers that are subject to thermal fluctuations are modeled using principles from statistical physics. In its simplest form, a polymer is modeled as an *ideal chain*, where interactions between chain segments are ignored. The *no-interaction* assumption allows the chain segments to cross each other in space and thus these chains are often called *phantom chains* [14]. In this section, we give a brief introduction to two types of ideal chains.

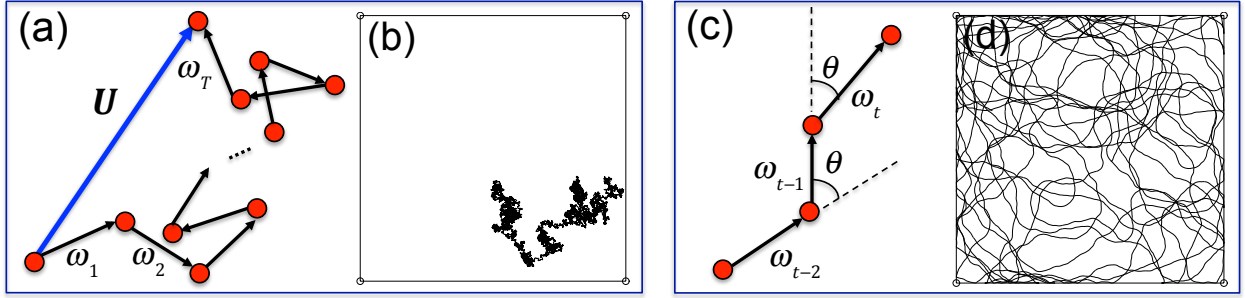


Figure 7: A chain (or trajectory) is shown as a sequence of T random bond vectors $\{\omega_i\}_{i=1..T}$. In a freely-jointed chain (a), the orientation of the bond vectors are independent of one another. The end-to-end vector of the chain is depicted by U . In a freely-rotating chain (c), the correlation angle θ is invariant between every two consecutive bond vectors, which induces a finite stiffness in the chain. (b, d) A qualitative comparison between an FJC (b) and an FRC with $\theta \approx 5.7^\circ$ (d), in a 2D environment of size 400×400 for 20000 number of moves.

Two main ideal chain models are: 1) freely-jointed chains (FJC) and 2) freely-rotating chains (FRC) [14]. In these models, chains of size T are demonstrated as a sequence of T random vectors $\{\omega_i\}_{i=1..T}$, which are as well called *bond vectors* (See Fig. 7). FJC is the simplest proposed model and is composed of mutually independent random vectors of the same size (Fig. 7(a)). In other words, an FJC chain is formed via uniform random sampling of vectors in space, and thus is a *random walk* (RW). In the FRC model, on the other hand, the notion of *correlation angle* is introduced, which is the angle θ between every two consecutive bond vectors. The FRC model, fixes the correlation angle θ (Fig. 7(c)), thus the vectors in the chain are temporally correlated. The vector sampling strategy in the FRCs induces *persistent chains*, in the sense that the orientation of the consecutive vectors in the space are preserved for certain number of time steps (a.k.a. persistence number), after which the correlation is broken and the bond vectors *forget* their original orientation. This feature introduces a finite *stiffness* in the chain, which induces what we call *local self avoidance*, leading to faster expansion of the chain in the space (Compare figures 7 (b) and (d) together). Below, we discuss two important properties of the FJCs and the FRCs, and subsequently formally introduce the *locally self-avoiding random walks* (LSA-RWs) in Definition 1.

FJCs (Property) - In the Freely-Jointed Chains (FJCs) or the flexible chains model, the orientations of the bond vectors in the space are mutually independent. To measure the expected end-to-end length of a chain \tilde{U} with T bond vectors of constant length b_o given the end-to-end vector $U = \sum_{i=1}^T \omega_i$ (Figure 7 (a)) and considering the mutual independence between bond vectors of an FJC, we can write [14],

$$\langle \|U\|^2 \rangle = \sum_{i,j=1}^T \langle \omega_i \cdot \omega_j \rangle = \sum_{i=1}^T \langle \omega_i^2 \rangle + 2 \sum_{i>j} \langle \omega_i \cdot \omega_j \rangle = T b_o^2, \quad (14)$$

where $\langle \cdot \rangle$ denotes the ensemble average over all possible conformations of the chain as a result of thermal fluctuations. Equation 14 shows that the expected end-to-end length $\tilde{U} = \langle \|U\|^2 \rangle^{1/2} = b_o \sqrt{T}$, which reveals random-walk behaviour as expected.

FRCs (Property) - In the Freely-Rotating Chains (FRCs) model, we assume that the angle θ (correlation angle) between every two consecutive bond vectors is invariant (Figure 7 (c)). Therefore, bond vectors $\omega_{i:1,\dots,T}$ are not mutually independent. Unlike the FJC model, in the FRC model the bond vectors are correlated such that [14],

$$\langle \omega_i \cdot \omega_j \rangle = b_o^2 (\cos \theta)^{|i-j|} = b_o^2 e^{-\frac{|i-j|}{L_p}}, \quad (15)$$

where $L_p = \frac{1}{|\log(\cos \theta)|}$ is the correlation length (persistence number). Equation 15 shows that the correlation between bond vectors in an FRC is a decaying exponential with correlation length L_p .

Lemma 6. [14] *Given an FRC characterized by end-to-end vector U , bond-size b_o and number of bond vectors T , we have $\langle \|U\|^2 \rangle = b^2 T$, where $b^2 = b_o^2 \frac{1+\cos \theta}{1-\cos \theta}$ and b is called the effective bond length.*

Lemma 6 shows that FRCs obey random walk statistics with step-size (bond length) $b > b_o$. The ratio $b/b_o = \frac{1+\cos \theta}{1-\cos \theta}$ is a measure of the stiffness of the chain in an FRC.

FRCs have high expansion rates compared to those of FJCs, as presented in Proposition 7 below.

Proposition 7 (Expanding property of LSA-RW). [14] *Let τ be a LSA-RW with the persistence number $L_{p\tau} > 1$ and the end-to-end vector $U(\tau)$, and let τ' be a random walk (RW) and the end-to-end vector $U(\tau')$. Then for the same number of time steps and same average bond length for τ and τ' , the following relation holds,*

$$\frac{\langle \|U(\tau)\| \rangle}{\langle \|U(\tau')\| \rangle} = \frac{1 + e^{-1/L_{p\tau}}}{1 - e^{-1/L_{p\tau}}} > 1, \quad (16)$$

where the persistence number $L_{p\tau} = \frac{1}{|\log \cos \theta|}$, with θ being the average correlation angle between every two consecutive bond vectors.

Proof. This proposition is the direct result of combining equations 2.7 and 2.14 in [14]. Equation 2.7 provides the expected T time-step length of the end-to-end vector with average step-size b_o associated with FJCs and equation 2.14 provides a similar result for FRCs. Note that in the FRC model, since the bond vectors far separated in time on the chain are not correlated, they can cross each other. \square

Radius of Gyration (Formal Definition) [43] The square radius of gyration $U_g^2(\tau)$ of a chain τ of size T is defined as the mean square distance between position vectors $t \in \tau$ and the chain center of mass ($\bar{\tau}$), and is written as,

$$U_g^2(\tau) := \frac{1}{T} \sum_{i=1}^T \|t_i - \bar{\tau}\|^2, \quad (17)$$

where $\bar{\tau} = \frac{1}{T} \sum_{i=1}^T t_i$. When it comes to selecting a measure of coverage in the space where the chain resides, radius of gyration U_g is a more proper choice compared with the end-to-end distance $\|U\|$, as it signifies the size of the chain with respect to its center of mass, and is proportional to the radius of the sphere (or the hyper sphere) that the chain occupies. Moreover, in the case of chains that are circular or branched, and thus cannot be assigned an end-to-end length, radius of gyration proves to be a suitable measure for the size of the corresponding chains [43]. For the case of fluctuating chains, the square radius of gyration is usually ensemble averaged over all possible chain conformations, and is written as [43],

$$\langle U_g^2(\tau) \rangle := \frac{1}{T} \sum_{i=1}^T \langle \|t_i - \bar{\tau}\|^2 \rangle. \quad (18)$$

Remark 1. The square radius of gyration U_g^2 is proportional to the square end-to-end distance $\|U\|^2$ in ideal chains (e.g. FJCs and FRCs) with a constant factor [43]. Thus, Proposition 7 and equation 16, which compare the end-to-end distance of LSA-RW and RW with each other, similarly hold for the radius of gyration of the respective models, implying faster expansion of the volume occupied by LSA-RW compared with that of RW.

B The Proofs

In this section, the proofs for the theorems and the lemma in the manuscript are provided.

B.1 The proof of Lemma 2 in the manuscript

Lemma 2 statement: Let $\tau_S = (s_0, \dots, s_{T-1})$ be the trajectory of visited states, s_T be a newly visited state and $\omega_i = s_i - s_{i-1}$ be the bond vector that connects two consecutive visited states s_{i-1} and s_i . Then we have,

$$\|s_T - \bar{\tau}_S\|^2 = \|\omega_T + \frac{1}{T} \left[\sum_{i=1}^{T-1} i\omega_i \right]\|^2. \quad (19)$$

Proof. Using the relation $\bar{\tau}_S := \frac{1}{T} \sum_{s \in \tau_S} s$ as well as the definition of bond vectors (equation (3) in the manuscript), we can write $s_T - \bar{\tau}_S$ on the left-hand side of equation (6) in the manuscript as,

$$\begin{aligned} s_T - \bar{\tau}_S &= s_T - \frac{1}{T} \sum_{s \in \tau_S} s \\ &= s_T - s_{T-1} + s_{T-1} - \frac{1}{T} \sum_{s \in \tau_S} s \\ &= \omega_T + \frac{1}{T} (s_{T-1} - s_0) + (s_{T-1} - s_1) + (s_{T-1} - s_2) + \dots \\ &\quad + (s_{T-1} - s_{T-2}) \\ &= \omega_T + \frac{1}{T} [(s_{T-1} - s_{T-2} + s_{T-2} - s_{T-3} + \dots \\ &\quad + s_2 - s_1 + s_1 - s_0) + (s_{T-1} - s_{T-2} + s_{T-2} - s_{T-3} + \dots \\ &\quad + s_3 - s_2 + s_2 - s_1) + \dots + (s_{T-1} - s_{T-2})] \\ &= \omega_T + \frac{1}{T} [(\omega_{T-1} + \dots + \omega_1) + (\omega_{T-1} + \dots + \omega_2) + \dots + \omega_{T-1}] \\ &= \omega_T + \frac{1}{T} \left[\sum_{i=1}^{T-1} i\omega_i \right] \end{aligned} \quad (20)$$

$$\Rightarrow \|s_T - \bar{\tau}_S\|^2 = \|\omega_T + \frac{1}{T} \left[\sum_{i=1}^{T-1} i\omega_i \right]\|^2 \quad (21)$$

□

B.2 The proof of Theorem 3 in the manuscript

Theorem 3 statement (Upper-Bound Theorem) Let $\delta \in (0, 1)$ and τ_S be a LSA-RW in \mathcal{S} induced by PolyRL with the persistence number $Lp_{\tau_S} > 1$ within episode N , $\omega_{\tau_S} = \{\omega_i\}_{i=1}^{T-1}$ be the sequence of corresponding bond vectors, where $T > 0$ denotes the number of bond vectors within τ_S , and b_o be the average bond length. The upper confidence bound for $ULS_{Ug^2}(\tau_S)$ with probability of at least $1 - \delta$ is,

$$UB = \Lambda(T, \tau_S) + \frac{1}{\delta} \left[\Gamma(T, b_o, \tau_S) + \frac{2b_o^2}{T^2} \sum_{i=1}^{T-1} i e^{\frac{-(T-i)}{Lp_{\tau_S}}} \right], \quad (22)$$

where,

$$\Lambda(T, \tau_S) = -\frac{1}{T-1} U_g^2(\tau_S) \quad (23)$$

$$\Gamma(T, b_o, \tau_S) = \frac{b_o^2}{T} + \frac{\|\sum_{i=1}^{T-1} i\omega_i\|^2}{T^3} \quad (24)$$

Proof. If we replace the term $U_g^2(\tau'_S)$ in equation (5) in the manuscript with its incremental representation as a function of $U_g^2(\tau_S)$, we get

$$\begin{aligned} UL S U_g^2(\tau_S) &= \sup_{s_T \in \Omega} \left(\frac{T-2}{T-1} U_g^2(\tau_S) + \frac{1}{T} \|s_T - \bar{\tau}_S\|^2 - U_g^2(\tau_S) \right) \\ &= -\frac{1}{T-1} U_g^2(\tau_S) + \sup_{s_T \in \Omega} \frac{1}{T} \|s_T - \bar{\tau}_S\|^2. \end{aligned} \quad (25)$$

Therefore, the problem reduces to the calculation of

$$\frac{1}{T} \sup_{s_T \in \Omega} \|s_T - \bar{\tau}_S\|^2. \quad (26)$$

Using Lemma 2 in the manuscript, we can write equation (26) in terms of bond vectors $\omega_i = s_i - s_{i-1}$ as,

$$\frac{1}{T} \sup_{s_T \in \Omega} \|s_T - \bar{\tau}_S\|^2 = \frac{1}{T} \sup_{s_T \in \Omega} \left\| \omega_T + \frac{1}{T} \left[\sum_{i=1}^{T-1} i \omega_i \right] \right\|^2. \quad (27)$$

From now on, with a slight abuse of notation, we will treat $\omega_T = S_T - s_{T-1}$ as a random variable due to the fact that S_T is a random variable in our system. Note that ω_i for $i = 1, 2, \dots, T-1$ is fixed, and thus is not considered a random variable. We use high-probability concentration bound techniques to calculate equation (26). For any $\delta \in (0, 1)$, there exists $\alpha > 0$, such that

$$\Pr \left[\left\| \omega_T + \frac{1}{T} \left[\sum_{i=1}^{T-1} i \omega_i \right] \right\|^2 < \alpha | S_T \in \Omega \right] > 1 - \delta. \quad (28)$$

We can rearrange equation 28 as,

$$\Pr \left[\left\| \omega_T + \frac{1}{T} \left[\sum_{i=1}^{T-1} i \omega_i \right] \right\|^2 \geq \alpha | S_T \in \Omega \right] \leq \delta. \quad (29)$$

Multiplying both sides by T^2 and expanding the squared term in equation 29 gives,

$$\Pr \left[T^2 \|\omega_T\|^2 + 2T(\omega_T \cdot \sum_{i=1}^{T-1} i \omega_i) + \left\| \sum_{i=1}^{T-1} i \omega_i \right\|^2 \geq T^2 \alpha | S_T \in \Omega \right] \leq \delta. \quad (30)$$

By Markov's inequality we have,

$$\begin{aligned} &\Pr \left[T^2 \|\omega_T\|^2 + 2T(\omega_T \cdot \sum_{i=1}^{T-1} i \omega_i) + \left\| \sum_{i=1}^{T-1} i \omega_i \right\|^2 \geq T^2 \alpha \right] \\ &\leq \frac{\mathbb{E} \left[T^2 \|\omega_T\|^2 + 2T(\omega_T \cdot \sum_{i=1}^{T-1} i \omega_i) + \left\| \sum_{i=1}^{T-1} i \omega_i \right\|^2 \right]}{T^2 \alpha} = \delta \\ &\implies \alpha = \frac{1}{\delta T^2} \left[T^2 \mathbb{E} [\|\omega_T\|^2] + 2T \mathbb{E} \left[\omega_T \cdot \sum_{i=1}^{T-1} i \omega_i \right] + \left\| \sum_{i=1}^{T-1} i \omega_i \right\|^2 \right] \\ &\stackrel{\text{by Def. 1}}{\implies} \alpha = \frac{1}{\delta T^2} \left[T^2 b_o^2 + 2T \mathbb{E} \left[\omega_T \cdot \sum_{i=1}^{T-1} i \omega_i \right] + \left\| \sum_{i=1}^{T-1} i \omega_i \right\|^2 \right] \end{aligned}$$

Note that all expectations \mathbb{E} in the equations above are over the transition kernel \mathcal{P} of the MDP. Using the results from Lemma 3 below, we conclude the proof. \square

Lemma 3. Let τ_S denote the sequence of states observed by PolyRL and S_T be the new state visited by PolyRL. Assuming that $\tau'_S := (\tau_S, S_T)$ (equation 2 in the manuscript) follows the LSAW formalism with the persistence number $Lp_{\tau_S} > 1$, we have

$$\mathbb{E} \left[\omega_T \cdot \sum_{i=1}^{T-1} i \omega_i \right] = b_0^2 \sum_{i=1}^{T-1} i e^{\frac{-|T-i|}{Lp_{\tau_S}}} \quad (31)$$

Proof.

$$\mathbb{E} \left[\boldsymbol{\omega}_T \cdot \sum_{i=1}^{T-1} i \boldsymbol{\omega}_i \right] = \mathbb{E} \left[\sum_{i=1}^{T-1} i \boldsymbol{\omega}_T \cdot \boldsymbol{\omega}_i \right] = \sum_{i=1}^{T-1} i \mathbb{E} [\boldsymbol{\omega}_T \cdot \boldsymbol{\omega}_i]. \quad (32)$$

Here, the goal is to calculate the expectation in equation 32 under the assumption that τ'_S is LSAW with persistence number $Lp_{\tau_S} > 1$. Note that if τ'_S is LSAW and $Lp_{\tau_S} > 1$, the chain of states visited by PolyRL prior to visiting s_T is also LSAW with $Lp_{\tau_S} > 1$. Now we focus on the expectation in equation 32. We compute $\mathbb{E} [\boldsymbol{\omega}_T \cdot \boldsymbol{\omega}_i]$ using the LSAW formalism (Definition 1 in the manuscript) as following,

$$\mathbb{E} [\boldsymbol{\omega}_T \cdot \boldsymbol{\omega}_i] = b_0^2 e^{\frac{-|T-i|}{Lp_{\tau_S}}}$$

Therefore, we have,

$$\sum_{i=1}^{T-1} i \mathbb{E} [\boldsymbol{\omega}_T \cdot \boldsymbol{\omega}_i] = \sum_{i=1}^{T-1} i b_0^2 e^{\frac{-(T-i)}{Lp_{\tau_S}}} = b_0^2 \sum_{i=1}^{T-1} i e^{\frac{-(T-i)}{Lp_{\tau_S}}}$$

□

B.3 The proof of Theorem 4 in the manuscript

Theorem 4 statement (Lower-Bound Theorem) Let $\delta \in (0, 1)$ and τ_S be a LSA-RW in \mathcal{S} induced by PolyRL with the persistence number $Lp_{\tau_S} > 1$ within episode N , $\boldsymbol{\omega}_{\tau_S} = \{\boldsymbol{\omega}_i\}_{i=1}^{T-1}$ be the sequence of corresponding bond vectors, where $T > 0$ denotes the number of bond vectors within τ_S , and b_o be the average bond length. The lower confidence bound for $LLS_{Ug^2}(\tau_S)$ at least with probability $1 - \delta$ is,

$$LB = \Lambda(T, \tau_S) + (1 - \sqrt{2 - 2\delta}) \left[\Gamma(T, b_o, \tau_S) + \frac{(T-1)(T-2)}{T^2} b_0^2 e^{\frac{-|T-1|}{Lp_{\tau_S}}} \right], \quad (33)$$

where,

$$\Lambda(T, \tau_S) = -\frac{1}{T-1} U_g^2(\tau_S) \quad (34)$$

$$\Gamma(T, b_o, \tau_S) = \frac{b_o^2}{T} + \frac{\|\sum_{i=1}^{T-1} i \boldsymbol{\omega}_i\|^2}{T^3} \quad (35)$$

Proof. Using the definition of radius of gyration and letting $d = L_2$ -norm in equation (4) in the manuscript, we have

$$\begin{aligned} LLS_{Ug^2}(\tau_S) &= \inf_{s_T \in \Omega} \frac{T-2}{T-1} U_g^2(\tau_S) + \frac{1}{T} \|s_T - \bar{\tau}_S\|^2 - U_g^2(\tau_S) \\ &= -\frac{1}{T-1} U_g^2(\tau_S) + \inf_{s_T \in \Omega} \frac{1}{T} \|s_T - \bar{\tau}_S\|^2 \end{aligned} \quad (36)$$

To calculate the high-probability lower bound, first we use the result from Lemma 2 in the manuscript. Thus, we have

$$\inf_{s_T \in \Omega} \frac{1}{T} \|s_T - \bar{\tau}_S\|^2 = \frac{1}{T} \inf_{s_T \in \Omega} \left\| \boldsymbol{\omega}_T + \frac{1}{T} \left[\sum_{i=1}^{T-1} i \boldsymbol{\omega}_i \right] \right\|^2. \quad (37)$$

We subsequently use the second moment method and Paley–Zygmund inequality to calculate the high-probability lower bound. Let $Y = \left\| \boldsymbol{\omega}_T + \frac{1}{T} \left[\sum_{i=1}^{T-1} i \boldsymbol{\omega}_i \right] \right\|^2$, for the finite positive constants c_1 and c_2 we have,

$$\Pr[Y > c_2 \beta] \geq \frac{(1 - \beta)^2}{c_1} \quad (38)$$

where,

$$\begin{aligned} \mathbb{E}[Y^2] &\leq c_1 \mathbb{E}[Y]^2 \\ \mathbb{E}[Y] &\geq c_2. \end{aligned} \quad (39)$$

The goal is to find two constants c_1 and c_2 such that equation (39) is satisfied and then we find $\beta \in (0, 1)$ in equation (38) using δ . We start by finding c_2 ,

$$\begin{aligned}
\mathbb{E}[Y] &= \mathbb{E} \left[\left(\omega_T + \frac{1}{T} \left[\sum_{i=1}^{T-1} i \omega_i \right] s \right) \cdot \left(\omega_T + \frac{1}{T} \left[\sum_{i=1}^{T-1} i \omega_i \right] \right) \right] \\
&= \mathbb{E} \left[\|\omega_T\|^2 + \frac{2}{T} (\omega_T \cdot \sum_{i=1}^{T-1} i \omega_i) + \frac{1}{T^2} \left\| \sum_{i=1}^{T-1} i \omega_i \right\|^2 \right] \\
&= \mathbb{E} [\|\omega_T\|^2] + \frac{2}{T} \sum_{i=1}^{T-1} i \mathbb{E} [\omega_T \cdot \omega_i] + \frac{1}{T^2} \left\| \sum_{i=1}^{T-1} i \omega_i \right\|^2 \\
&= b_o^2 + \frac{2}{T} b_o^2 \sum_{i=1}^{T-1} i e^{\frac{-|T-i|}{L^p \tau_S}} + \frac{1}{T^2} \left\| \sum_{i=1}^{T-1} i \omega_i \right\|^2,
\end{aligned} \tag{40}$$

therefore,

$$\begin{aligned}
\mathbb{E}[Y] &= b_o^2 + \frac{2}{T} b_o^2 \sum_{i=1}^{T-1} i e^{\frac{-|T-i|}{L^p \tau_S}} + \frac{1}{T^2} \left\| \sum_{i=1}^{T-1} i \omega_i \right\|^2 \\
&\geq b_o^2 + \frac{2}{T} b_o^2 e^{\frac{-|T-1|}{L^p \tau_S}} \sum_{i=1}^{T-1} i + \frac{1}{T^2} \left\| \sum_{i=1}^{T-1} i \omega_i \right\|^2 \\
&= b_o^2 + \underbrace{\frac{(T-1)(T-2)}{T} b_o^2 e^{\frac{-|T-1|}{L^p \tau_S}} + \frac{1}{T^2} \left\| \sum_{i=1}^{T-1} i \omega_i \right\|^2}_{=c_2}
\end{aligned} \tag{41}$$

To find c_1 , we have

$$\mathbb{E}[Y^2] \leq c_1 \mathbb{E}[Y]^2.$$

$$\begin{aligned}
\mathbb{E}[Y^2] &= \mathbb{E} \left[\left(\|\omega_T\|^2 + \frac{2}{T} (\omega_T \cdot \sum_{i=1}^{T-1} i \omega_i) + \frac{1}{T^2} \left\| \sum_{i=1}^{T-1} i \omega_i \right\|^2 \right)^2 \right] \\
&= \mathbb{E} [\|\omega_T\|^4] + \frac{4}{T^2} \mathbb{E} \left[(\omega_T \cdot \sum_{i=1}^{T-1} i \omega_i)^2 \right] \\
&\quad + \frac{1}{T^4} \mathbb{E} \left[\left\| \sum_{i=1}^{T-1} i \omega_i \right\|^4 \right] + \frac{4}{T} \mathbb{E} \left[\|\omega_T\|^2 (\omega_T \cdot \sum_{i=1}^{T-1} i \omega_i) \right] \\
&\quad + \frac{2}{T^2} \mathbb{E} \left[\|\omega_T\|^2 \left\| \sum_{i=1}^{T-1} i \omega_i \right\|^2 \right] + \frac{2}{T^3} \mathbb{E} \left[(\omega_T \cdot \sum_{i=1}^{T-1} i \omega_i) \left\| \sum_{i=1}^{T-1} i \omega_i \right\|^2 \right] \\
&= \mathbb{E} [\|\omega_T\|^4] + \frac{4}{T^2} \mathbb{E} \left[(\omega_T \cdot \sum_{i=1}^{T-1} i \omega_i)^2 \right] \\
&\quad + \frac{1}{T^4} \left\| \sum_{i=1}^{T-1} i \omega_i \right\|^4 + \frac{4}{T} \mathbb{E} \left[\|\omega_T\|^2 (\omega_T \cdot \sum_{i=1}^{T-1} i \omega_i) \right] \\
&\quad + \frac{2b_o^2}{T^2} \left\| \sum_{i=1}^{T-1} i \omega_i \right\|^2 + \frac{2}{T^3} \left\| \sum_{i=1}^{T-1} i \omega_i \right\|^2 \mathbb{E} \left[(\omega_T \cdot \sum_{i=1}^{T-1} i \omega_i) \right]
\end{aligned} \tag{42}$$

We calculate the expectations appearing in equation (42) to conclude the proof.

$$\begin{aligned}
\frac{4}{T^2} \mathbb{E} \left[\left(\omega_T \cdot \sum_{i=1}^{T-1} i \omega_i \right)^2 \right] &\leq \frac{4}{T^2} \mathbb{E} \left[\left(\|\omega_T\| \left\| \sum_{i=1}^{T-1} i \omega_i \right\| \right)^2 \right] \\
&= \frac{4 \left\| \sum_{i=1}^{T-1} i \omega_i \right\|^2}{T^2} \mathbb{E} \left[(\|\omega_T\|)^2 \right] \\
&= \frac{4 \left\| \sum_{i=1}^{T-1} i \omega_i \right\|^2 b_o^2}{T^2}
\end{aligned} \tag{43}$$

$$\begin{aligned}
\frac{4}{T} \mathbb{E} \left[\|\omega_T\|^2 \left(\omega_T \cdot \sum_{i=1}^{T-1} i \omega_i \right) \right] &= \frac{4}{T} \mathbb{E} \left[\sum_{i=1}^{T-1} i \|\omega_T\|^2 \omega_T \cdot \omega_i \right] \\
&= \frac{4}{T} \sum_{i=1}^{T-1} i \mathbb{E} \left[\|\omega_T\|^2 \omega_T \cdot \omega_i \right] \\
&= \frac{4 \max_{s,s'} \|\omega(s, s')\|^2}{T} \sum_{i=1}^{T-1} i \mathbb{E} [\omega_T \cdot \omega_i] \\
&= \frac{4 b_o^2 \max_{s,s'} \|\omega(s, s')\|^2}{T} \sum_{i=1}^{T-1} i e^{\frac{-(T-i)}{L p \tau_S}}
\end{aligned} \tag{44}$$

where $\omega(s, s')$ denotes the bond vector between two states s and s' .

To calculate $\mathbb{E} [\|\omega_T\|^4]$, we let $Z \sim \mathcal{N}(0, 1)$ and using definition 1, w.l.o.g. we assume $\|\omega_T\|^2 \sim \mathcal{N}(b_o^2, \sigma^2)$ with $\sigma < \infty$. Thus, we have

$$\begin{aligned}
\mathbb{E} [\|\omega_T\|^4] &= \mathbb{E} [\sigma^2 Z^2 + 2b_o^2 \sigma Z + b_o^4] \\
&\quad \underbrace{=}_{\text{Binomial Theorem and linearity of expectation}} \sigma^2 + b_o^4
\end{aligned} \tag{45}$$

$$\mathbb{E} \left[\left(\omega_T \cdot \sum_{i=1}^{T-1} i \omega_i \right) \right] = \mathbb{E} \left[\left(\sum_{i=1}^{T-1} i \omega_T \cdot \omega_i \right) \right] = \sum_{i=1}^{T-1} i \mathbb{E} [\omega_T \cdot \omega_i] = \sum_{i=1}^{T-1} i b_o^2 e^{\frac{-(T-i)}{L p \tau_S}} \tag{46}$$

Substitution of the expectations in equation (42) with equations (45), (43), (44) and (46) gives,

$$\begin{aligned}
\mathbb{E} [Y^2] &\leq \sigma^2 + b_o^4 + \frac{4b_o^2}{T^2} \left\| \sum_{i=1}^{T-1} i \omega_i \right\|^2 + \frac{1}{T^4} \left\| \sum_{i=1}^{T-1} i \omega_i \right\|^4 + \frac{4b_o^2 \max_{s,s'} \|\omega(s, s')\|^2}{T} \sum_{i=1}^{T-1} i e^{\frac{-(T-i)}{L p \tau_S}} \\
&\quad + \frac{2b_o^2}{T^2} \left\| \sum_{i=1}^{T-1} i \omega_i \right\|^2 + \frac{2b_o^2}{T^3} \sum_{i=1}^{T-1} i e^{\frac{-(T-i)}{L p \tau_S}} \left\| \sum_{i=1}^{T-1} i \omega_i \right\|^2
\end{aligned} \tag{47}$$

Equation (40) gives,

$$\begin{aligned}
\mathbb{E} [Y]^2 &= b_o^4 + \frac{4b_o^4}{T^2} \left(\sum_{i=1}^{T-1} i e^{\frac{-(T-i)}{L p \tau_S}} \right)^2 + \frac{1}{T^4} \left\| \sum_{i=1}^{T-1} i \omega_i \right\|^4 + \frac{2b_o^4}{T^2} \sum_{i=1}^{T-1} i e^{\frac{-(T-i)}{L p \tau_S}} \\
&\quad + \frac{2b_o^2}{T^2} \left\| \sum_{i=1}^{T-1} i \omega_i \right\|^2 + \frac{2b_o^2}{T^3} \sum_{i=1}^{T-1} i e^{\frac{-(T-i)}{L p \tau_S}} \left\| \sum_{i=1}^{T-1} i \omega_i \right\|^2
\end{aligned} \tag{48}$$

Now to find c_1 , we use equation (39),

$$\begin{aligned} \frac{4b_o^2}{T^2} \left\| \sum_{i=1}^{T-1} i\omega_i \right\|^2 - \frac{4b_o^4}{T^2} \left(\sum_{i=1}^{T-1} ie^{\frac{-|T-i|}{Lp_{\tau_S}}} \right)^2 &= \frac{4b_o^2}{T^2} \left(\left\| \sum_{i=1}^{T-1} i\omega_i \right\|^2 - \left(\sum_{i=1}^{T-1} ie^{\frac{-|T-i|}{Lp_{\tau_S}}} \right)^2 \right) \\ &\leq \underbrace{\frac{4b_o^2}{T^2} \left(\left\| \sum_{i=1}^{T-1} i\omega_i \right\|^2 \right)}_B. \end{aligned}$$

$$\begin{aligned} &\frac{4b_o^2 \max_{s,s'} \|\omega(s, s')\|^2}{T} \sum_{i=1}^{T-1} ie^{\frac{-(T-i)}{Lp_{\tau_S}}} - \frac{2b_o^4}{T^2} \sum_{i=1}^{T-1} ie^{\frac{-(T-i)}{Lp_{\tau_S}}} \\ &= \left(\frac{4b_o^2 \max_{s,s'} \|\omega(s, s')\|^2}{T} - \frac{2b_o^4}{T^2} \right) \sum_{i=1}^{T-1} ie^{\frac{-(T-i)}{Lp_{\tau_S}}} \\ &\leq \underbrace{\left(\frac{4b_o^2 \max_{s,s'} \|\omega(s, s')\|^2}{T} \right) \sum_{i=1}^{T-1} ie^{\frac{-(T-i)}{Lp_{\tau_S}}}}_A \end{aligned}$$

Thus, we have

$$\frac{\mathbb{E}[Y^2]}{\mathbb{E}[Y]^2} \leq 1 + \frac{\sigma^2 + A + B}{\mathbb{E}[Y]^2} \underbrace{\leq}_{\text{by comparing A and B with (48)}} 2 = c_1 \quad (49)$$

□

B.4 The proof of Corollary 5 in the manuscript

Corollary 5 statement: Given that assumption 1 in the manuscript is satisfied, with high probability the exploratory trajectories formed in \mathcal{S} induced by PolyRL Algorithm (Algorithm 1 in the manuscript) are LSA-RWs.

Proof. Given Assumption 1 in the manuscript, due to the Lipschitzness of the transition probability kernel w.r.t. the action variable, the change in the distributions of the resulting states are finite and bounded by the L_2 distance of the actions. Thus, given a locally self-avoiding chain $\tau_A \in \mathcal{A}^T$ with persistence number Lp_{τ_A} , and $\forall i \in [T] : b_o^2 = \langle \|a_i\|^2 \rangle$, by the Lipschitzness of the transition probability kernel of the underlying MDP, there exists a finite empirical average bond vector among the states visited by PolyRL (*i.e.* the first condition in Definition 1 in the manuscript is satisfied).

On the other hand, the PolyRL action sampling method (Algorithm 2) by construction preserves the expected correlation angle θ_{τ_A} between the consecutive selected actions with finite L_2 norm, leading to a locally self-avoiding random walk in \mathcal{A} . Given the following measure of spread adopted by PolyRL and defined as,

$$U_g^2(\tau_S) := \frac{1}{T-1} \sum_{s \in \tau_S} \|s - \bar{\tau}_S\|^2, \quad (50)$$

and the results of Theorems 3 and 4 in the manuscript (LB and UB high probability confidence bounds on the sensitivity of $U_g^2(\cdot)$), and considering that at each time step the persistence number of the chain of visited states Lp_{τ_S} is calculated and the exploratory action is selected such that the stiffness of τ_S is preserved, with probability $1 - \delta$ the correlation between the bonds in τ_S is maintained (*i.e.* the second condition in Definition 1 in the manuscript is satisfied). Hence, with probability $1 - \delta$ the chain τ_S induced by PolyRL is locally self avoiding. □

Corollary 8. Under assumption 1 in the manuscript, with high probability the T time-step exploratory chain τ induced by PolyRL with persistence number Lp_τ provides higher space coverage compared with the T time-step exploratory chain τ' generated by a random-walk model.

Proof. Results from Corollary 5 in the manuscript together with remark 1 conclude the proof. □

C Action Sampling Method

In this section, we provide the action sampling algorithm 2, which contains the step-by-step instruction for sampling the next action. The action sampling process is also graphically presented in figure 8 (a).

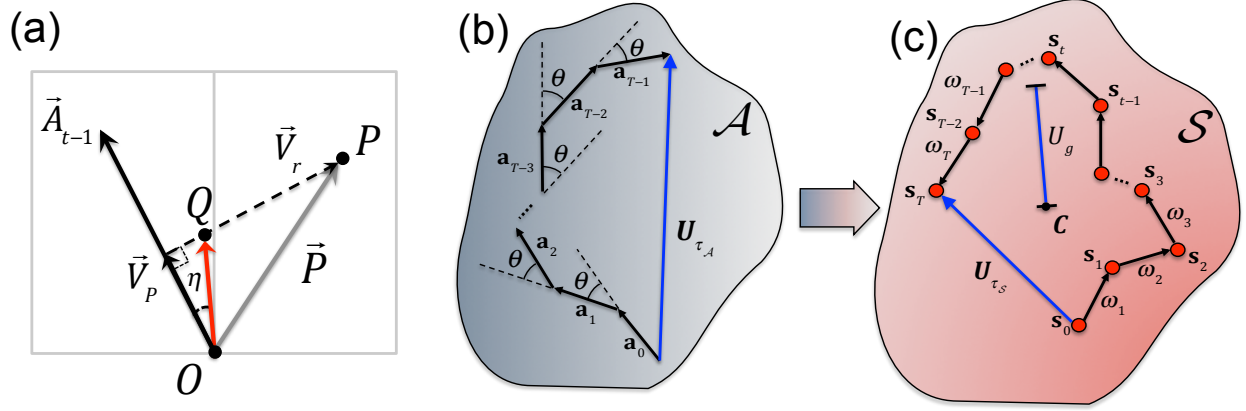


Figure 8: Schematics of the steps involved in the PolyRL exploration technique. (a) The action sampling method. In order to choose the next action \vec{A}_t , a randomly chosen point P in \mathcal{A} is projected onto the current action vector \vec{A}_{t-1} , which gives \vec{V}_P . The point Q is subsequently found on the vector $\vec{V}_r = \vec{P} - \vec{V}_P$ using trigonometric relations and the angle η drawn from a normal distribution with mean θ . The resulting vector \vec{OQ} (shown in red) gives the next action. Detailed instructions are given in Algorithm 2. (b) A schematic of action trajectory τ_A with the mean correlation angle θ between every two consecutive bond vectors and the end-to-end vector \vec{U}_{τ_A} . (c) A schematic of state trajectory τ_S with bond vectors $\omega_i = s_i - s_{i-1}$. The radius of gyration and the end-to-end vector are depicted as U_g and \vec{U}_{τ_S} , respectively. Point C is the center of mass of the visited states.

Algorithm 2 Action Sampling

Require: Angle η and Previous action \mathbf{A}_{t-1}

- 1: Draw a random point P in the action space ($P_i \sim \mathcal{U}[-m, m]; i = 1, \dots, d$) $\triangleright \mathbf{P}$ is the vector from the origin to the point P
 - 2: $D = \mathbf{A}_{t-1} \cdot \mathbf{P}$
 - 3: $\mathbf{V}_p = \frac{D}{\|\mathbf{A}_{t-1}\|_2^2} \mathbf{A}_{t-1}$ \triangleright The projection of \mathbf{P} on \mathbf{A}_{t-1}
 - 4: $\mathbf{V}_r = \mathbf{P} - \mathbf{V}_p$
 - 5: $l = \|\mathbf{V}_p\|_2 \tan \eta$
 - 6: $k = l / \|\mathbf{V}_r\|_2$
 - 7: $\mathbf{Q} = k \mathbf{V}_r + \mathbf{V}_p$
 - 8: **if** $D > 0$ **then**
 - 9: $\mathbf{A}_t = \mathbf{Q}$
 - 10: **else**
 - 11: $\mathbf{A}_t = -\mathbf{Q}$
 - 12: **end if**
 - 13: Clip \mathbf{A}_t if out of action range
 - 14: **return** \mathbf{A}_t
-

D Additional Baseline Results

In this section, we provide the benchmarking results for DDPG-UC, DDPG-OU, DDPG-PARAM (Figure 9), and SAC (Figure 10) algorithms on three standard MuJoCo tasks. Moreover, the source code is provided [here](#).

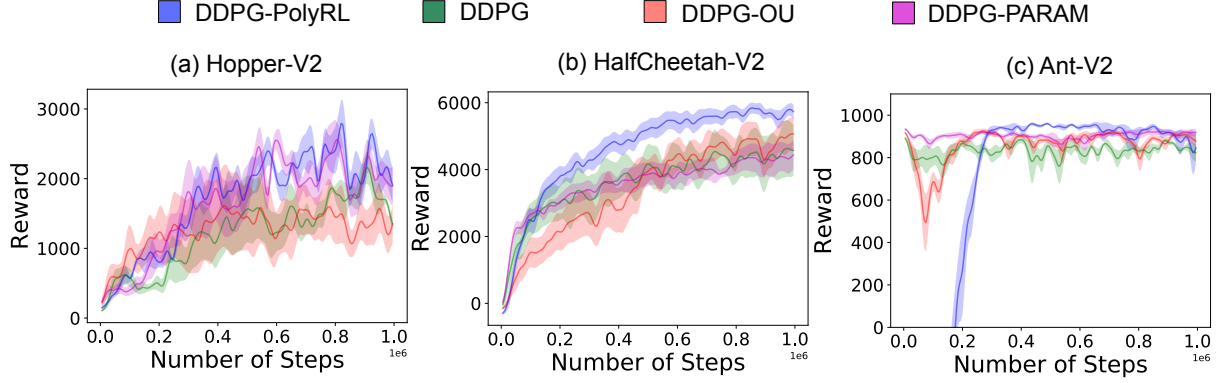


Figure 9: Performance of DDPG-UC, DDPG-OU, and DDPG-PARAM algorithms across 3 MuJoCo domains. The plots are averaged over 5 random seeds. The test evaluation happens every 5k over 1 million time-steps.

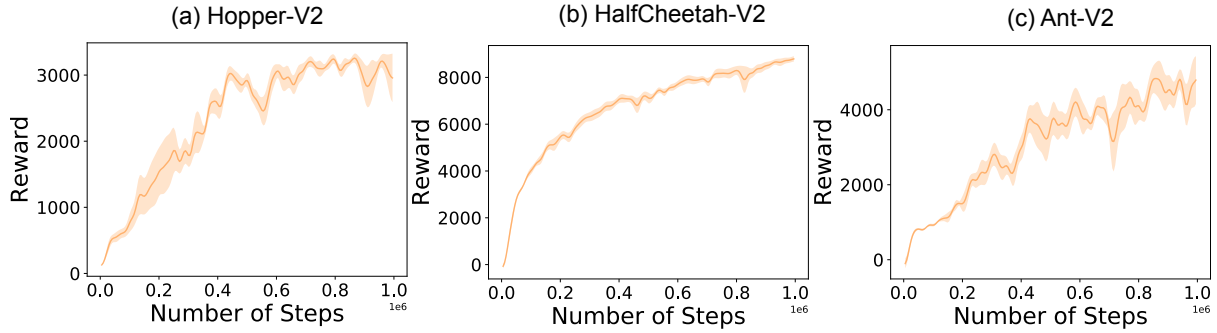


Figure 10: Performance of SAC algorithm across 3 MuJoCo domains. The plots are averaged over 5 random seeds. The test evaluation happens every 5k steps over 3 million time-steps.

E Hyperparameters and Network Architecture

In this section, we provide the architecture of the neural networks (Table 1), as well as the PolyRL hyper parameters (Table 2) used in the experiments. Regarding the computing infrastructure, the experiments were run on a slurm-managed cluster with NVIDIA P100 Pascal (12G HBM2 memory) GPUs. The average run-time for DDPG-based and SAC-based models were around 8 and 12 hours, respectively.

Table 1: DDPG and SAC Network Architecture

Parameter	Value	
Optimizer	Adam	
Critic Learning Rate	1e−3 (DDPG)	3e−4 (SAC)
Actor Learning Rate	1e−4 (DDPG)	3e−4 (SAC)
Discount Factor	0.99	
Replay Buffer Size	1e+6	
Number of Hidden Layers (All Networks)	2	
Number of Units per Layer	400 (1 st)- 300 (2 nd) (DDPG)	both 256 (SAC)
Number of Samples per Mini Batch	100	
Nonlinearity	ReLU	
Target Network Update Coefficient	5e−3	
Target Update Interval	1	

The exploration factor - The one important parameter in the PolyRL exploration method, which controls the exploration-exploitation trade-off is the exploration factor $\beta \in [0, 1]$. The factor β plays the balancing role in two ways: controlling (1) the range of confidence interval (equations (7) and (9) in the manuscript; $\delta = 1 - e^{-\beta N}$); and (2) the probability of switching from the target policy π_μ to the behaviour policy π_{PolyRL} . Figure 11 illustrates the effect of varying β on the performance of a DDPG-PolyRL agent in the HalfCheetah-v2 environment. The heat maps (Figures 11 (a), (b) and (c)) show the average asymptotic reward obtained for different pairs of correlation angle θ and variance σ^2 . The heat maps depict that for this specific task, the performance of DDPG-PolyRL improves as β changes from 0.0004 to 0.01. The performance plot for the same task (Figure 11 (d)) shows the effect of β on the amount of the obtained reward. The relation of β with the percentage of the moves taken using the target policy is illustrated in Figure 11 (e)). As expected, larger values of β lead to more exploitation and fewer exploratory steps.

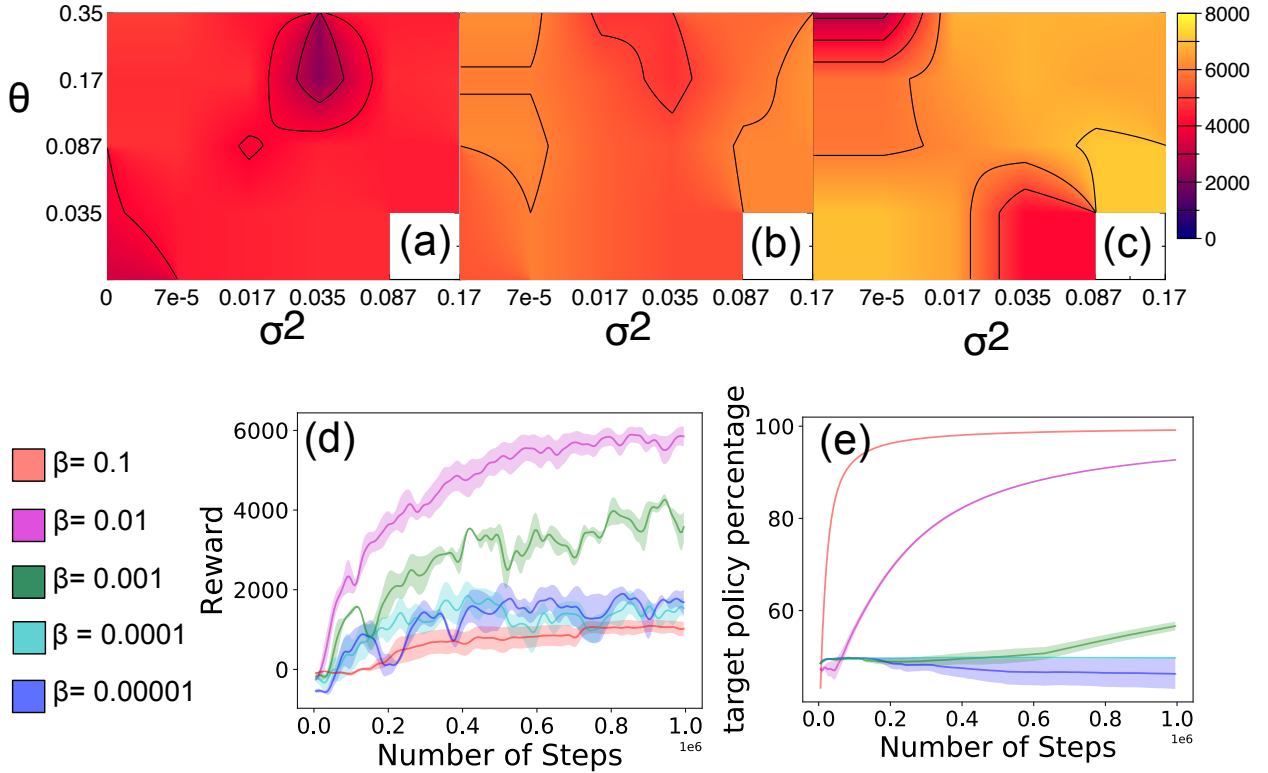


Figure 11: Performance of DDPG-PolyRL in HalfCheetah-v2 for different values of exploration factor β . (a-c) Heat maps depict the mean of the obtained asymptotic rewards after 3 million time steps over a range of correlation angle θ and the variance σ^2 . The results are shown for $\beta = 0.0004$ (a), $\beta = 0.001$ (b), and $\beta = 0.01$ (c). (d) Performance of DDPG-PolyRL in HalfCheetah-v2 for the fixed values of $\theta = 0.035$ and $\sigma^2 = 0.00007$, and different values of β . (e) The percentage of the movements the DDPG-PolyRL agent behaves greedily. All values are averaged over four random seeds and the error bars show the standard error on the mean.

Table 2: PolyRL Hyper parameters. Note that the parameters θ and σ are angles and their respective values in the table are in radian.

	Mean Correlation Angle θ	Variance σ^2	Exploration Factor β
<i>DDPG-PolyRL</i>			
<i>SparseHopper-V2</i> ($\lambda = 0.1$)	0.035	0.00007	0.001
<i>SparseHalfCheetah-V2</i> ($\lambda = 5$)	0.17	0.017	0.02
<i>SparseAnt-V2</i> ($\lambda = 0.15$)	0.087	0.035	0.01
<i>SAC-PolyRL</i>			
<i>SparseHopper-V2</i> ($\lambda = 3$)	0.35	0.017	0.01
<i>SparseHalfCheetah-V2</i> ($\lambda = 15$)	0.35	0.00007	0.05
<i>SparseAnt-V2</i> ($\lambda = 3$)	0.035	0.00007	0.01